

Classical correlated imaging from the perspective of coherent-mode representation

Jing Cheng¹ and Shensheng Han²

¹*School of Physical Science and Technology, South China University of Technology, Guangzhou 510640, China*

²*Key Laboratory for Quantum Optics and Center for Cold Atom Physics, Shanghai Institute of Optics and Fine Mechanics, Chinese Academy of Sciences, Shanghai 201800, China*

(Received 26 January 2007; revised manuscript received 29 April 2007; published 27 August 2007)

We use coherent-mode representation of partially coherent fields to analyze correlated imaging with classical light sources. This formalism is very useful to study the imaging quality. By decomposing the unknown object as the superposition of different coherent modes, the components corresponding to small eigenvalues cannot be well imaged. The generated images depend crucially on the distribution of the eigenvalues of the coherent-mode representation of the source and the decomposition coefficients of the objects. Three kinds of correlated imaging schemes are analyzed numerically.

DOI: [10.1103/PhysRevA.76.023824](https://doi.org/10.1103/PhysRevA.76.023824)

PACS number(s): 42.25.Kb, 42.30.Va, 42.50.Ar

I. INTRODUCTION

Correlated imaging, also known as ghost imaging or coincidence imaging, attracts much attention in recent years [1–17]. In a correlated imaging experiment, by correlating the intensity fluctuations of two spatially correlated beams that travel through two different imaging systems, an unknown object in one of the imaging systems can be nonlocally retrieved on the detector of the other imaging system. Though the experimental demonstration of correlated imaging was first realized with entangled photons generated by spontaneous down conversion [2,3], it is now widely accepted that both classical thermal sources and quantum entangled beams can be used for correlated imaging [1,6–10]. Classical correlated imaging experiments have been successfully demonstrated with both pseudothermal light and true thermal light [11–13]. Very recently, lensless ghost imaging [14,15] and lensless ghost diffraction [17] schemes have been demonstrated experimentally.

The present theory on classical correlated imaging is based on the integral representation, which have been derived from both quantum optics and statistical optics [6–8]. In the second order coherence theory of optical fields [18], it is well known that the cross-spectral density function of the source can be decomposed into a linear superposition of a series of coherent modes. In other words, if the source is quasimonochromatic, as in most experiments, there is also a decomposition of the second-order correlation function of the source into coherent modes. In this paper, we use the coherent-mode representation of partially coherent fields to analyze correlated imaging with a classical light source. This method is particularly suitable for evaluating the imaging quality and retrieving unknown information.

The paper is organized as follows. In Sec. II, we give the theoretical formulas and use them to analyze three kinds of correlated imaging schemes. Then numerical examples are simulated and discussed in Sec. III. Finally, conclusions are presented in Sec. IV.

II. THEORY

A simplified classical correlated imaging system is shown in Fig. 1. A partially coherent classical beam is divided into

two correlated beams by the beam splitter BS. These two beams then propagate through two different imaging systems, characterized by their impulse response functions $h_t(x_1, y_t)$, $h_r(x_2, y_r)$. An unknown object is included in the test system h_t , while the reference system h_r is fully known. By measuring the correlation function of intensity fluctuations in two different detectors D_t and D_r , we can retrieve the image of the object, which is proportional to [6–8]

$$G(y_r, y_t) = \langle \Delta I_r(y_r) \Delta I_t(y_t) \rangle = \left| \int dx_1 dx_2 \Gamma(x_1, x_2) h_t^*(x_1, y_t) h_r(x_2, y_r) \right|^2, \quad (1)$$

where $\Gamma(x_1, x_2)$ is the second-order spatial correlation function of the quasimonochromatic source. $\langle \dots \rangle$ denotes the statistical average, and $\Delta I_k(y_k) = I_k(y_k) - \langle I_k(y_k) \rangle$, with $k=t$ or r . To avoid confusion, in this paper, we use symbol $x_{1,2}$ as the coordinates for the source, and $y_{r,t}$ as the coordinates for the detectors.

From the optical coherence theory, $\Gamma(x_1, x_2)$ can be expressed in the coherent-mode representation [18]

$$\Gamma(x_1, x_2) = \sum_n \beta_n \phi_n^*(x_1) \phi_n(x_2), \quad (2)$$

where β_n are the eigenvalues and $\phi_n(x)$ are the eigenfunctions of the homogeneous Fredholm integral equation

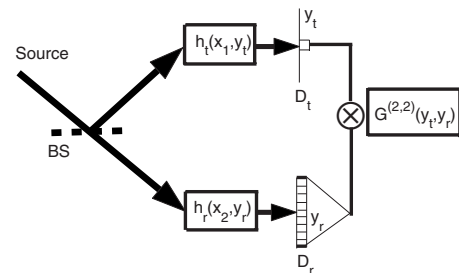


FIG. 1. A simplified classical correlated imaging system. A partially coherent source is split into two beams by the beam splitter BS. One transmits through the test system (h_t) and the other through the reference system (h_r). Two detectors D_t and D_r record the intensity distribution. A correlator is used to measure the correlation function of intensity fluctuations.

$$\int dx_1 \Gamma(x_1, x_2) \phi_n(x_1) = \beta_n \phi_n(x_2).$$

The eigenvalues are real and satisfy $\beta_0 \geq \beta_1 \dots \geq 0$, and the eigenfunctions form an orthonormal set,

$$\int dx \phi_n^*(x) \phi_m(x) = \delta_{nm}.$$

Now, we use the coherent-mode representation to analyze the correlated imaging schemes. Substituting Eq. (2) into Eq. (1), we have

$$G(y_r, y_t) = \left| \int dx_1 dx_2 \sum_n \beta_n \phi_n^*(x_1) \phi_n(x_2) h_t^*(x_1, y_t) h_r(x_2, y_r) \right|^2 = \left| \sum_n \beta_n f_n^*(y_t) g_n(y_r) \right|^2, \quad (3)$$

where

$$f_n(y_t) = \int dx_1 h_t(x_1, y_t) \phi_n(x_1),$$

and

$$g_n(y_r) = \int dx_2 h_r(x_2, y_r) \phi_n(x_2). \quad (4)$$

Due to the orthonormal properties of $\phi_n(x)$, both h_t and h_r can be expanded as

$$h_t(x_1, y_t) = \sum_n f_n(y_t) \phi_n^*(x_1),$$

$$h_r(x_2, y_r) = \sum_n g_n(y_r) \phi_n^*(x_2). \quad (5)$$

Equation (3) is the key formula in this paper. The two-dimensional integral representation Eq. (1) is reduced to a one-dimensional summation representation Eq. (3), which states that the image is the superposition of many coherent images. Since g_n is independent of the unknown object, $g_n(y_r)$ contains no information of the object, if only one coherent mode contributes significantly, then we cannot obtain an image of the object on the reference detector D_r . On the other hand, the superposition of a large number of coherent modes can provide enough information of the unknown object, then a nonlocal image of the object can be generated. In fact, if h_r has the unitary property, it is easy to show that $g_n(y_r)$ also form an orthonormal set. Thus, the greater the number of significant coherent modes, the more information about the object is contained in the correlated image. Further, since the image crucially relies on the distribution of the eigenvalues β_n , we find β_n plays the role of optical transfer function in the conventional imaging systems.

Now we use this new theory to analyze several typical examples of correlated imaging schemes: ghost diffraction [8,11], ghost imaging [8,11], and lensless ghost diffraction [6,17]. We show how the imaging quality relates to the coherent-mode representation of the source.

In the case of ghost diffraction, both the test and reference system are $2f$ imaging systems [8]. So we have

$$h_t(x_1, y_t) = t(x_1) \exp(-ix_1 y_t k/f),$$

$$h_r(x_2, y_r) = \exp(-ix_2 y_r k/f),$$

where $t(x_1)$ is the complex transmission function of the unknown object, $k=2\pi/\lambda$ is the wave number, and f is the focal length of the lens. By simple calculation, from Eq. (4), we find

$$g_n(y_r) = \int dx_2 \exp(-ix_2 y_r k/f) \phi_n(x_2) = \Phi_n(y_r k/f),$$

where $\Phi_n(q)$ is the Fourier transform of $\phi_n(x)$, then the correlated image (set $y_t=0$) is

$$G(y_r, 0) = \left| \sum_n \beta_n f_n^*(0) \Phi_n(y_r k/f) \right|^2. \quad (6)$$

According to Eq. (5),

$$t(x_1) = h_t(x_1, 0) = \sum_n f_n(0) \phi_n^*(x_1),$$

and its Fourier transform is

$$T(q) = \sum_n f_n(0) \Phi_n^*(-q),$$

so we have

$$T^*(-q) = \sum_n f_n^*(0) \Phi_n(q),$$

thus we see that the ghost diffraction [Eq. (6)] is a degraded image of the object's Fourier transform. The degraded degree crucially depends on the distribution of β_n . If all eigenvalues are equal, i.e., $\beta_n = \beta_0$, the object's Fourier transform can be perfectly imaged. If the distribution of β_n is sharply decreased, only a very limited number of the coherent-mode components of the object can be imaged, and the image will greatly deviate from the perfect pattern.

Secondly, we study the case of ghost imaging. In this example, the test system is not changed, while the reference system is replaced by a $4f$ imaging system [8],

$$h_r(x_2, y_r) = \delta(x_2 + y_r) \exp(-ik|x_2|^2/2f).$$

Then from Eq. (4), we have

$$g_n(y_r) = \int dx_2 \delta(x_2 + y_r) \exp(-ik|x_2|^2/2f) \phi_n(x_2) = \phi_n(-y_r) \exp(-ik|y_r|^2/2f),$$

and the correlated image (set $y_t=0$) is

$$G(y_r, 0) = \left| \sum_n \beta_n f_n^*(0) \phi_n(-y_r) \right|^2. \quad (7)$$

Since

$$t(-x_1)^* = h_t(-x_1, 0)^* = \sum_n f_n(0)^* \phi_n(-x),$$

we see a degraded image of the object is generated. For very small eigenvalues, the corresponding components of the object $f_n^*(0)\phi_n(-y_r)$ cannot be well imaged. But for those $\beta_n \approx \beta_0$, the corresponding components of the object can be imaged perfectly well.

In the third case, we analyze the lensless ghost diffraction scheme [6,17]. Here, only free-space Fresnel diffractions are considered as follows:

$$h_t(x_1, y_r) = t(x_1) \exp[-i\pi(x_1 - y_r)^2/\lambda z],$$

$$h_r(x_2, y_r) = \exp[-i\pi(x_2, y_r)^2/\lambda z].$$

From Eq. (5),

$$h_t(x_1, 0) = t(x_1) \exp[-i\pi(x_1)^2/\lambda z] = \sum_n f_n(0) \phi_n^*(x_1),$$

then

$$t(x_1) = \sum_n f_n(0) \phi_n^*(x_1) \exp(i\pi x_1^2/\lambda z),$$

so the ghost image (set $y_r=0$) is

$$G(y_r, 0) = \left| \sum_n \beta_n f_n^*(0) \int dx_2 \phi_n(x_2) e^{-i\pi x_2^2/\lambda z} e^{i\pi x_2 y_r/kz} \right|^2. \quad (8)$$

Compared with

$$T(q) = \sum_n f_n(0) \int dx_1 \phi_n^*(x_1) e^{i\pi x_1^2/\lambda z} e^{-i\pi x_1 q},$$

we can see in the lensless ghost diffraction scheme, the correlated image is also a degraded image of the object's Fourier transform, and the degradation is also determined by β_n .

III. NUMERICAL RESULTS

In this section, numerical examples are given to demonstrate our theoretical analysis. The source is supposed to be described by the Gaussian Schell model,

$$\Gamma(x_1, x_2) = \exp\left(-\frac{x_1^2 + x_2^2}{4\sigma_s^2}\right) \exp\left(-\frac{(x_1 - x_2)^2}{2\sigma_g^2}\right), \quad (9)$$

where σ_s and σ_g are two parameters to characterize the size and the coherence of the source. The coherent-mode representation of such a kind of Gaussian Schell-model source has been given in literatures [18]. The normalized eigenfunctions and the eigenvalues are

$$\phi_n(x) = \left(\frac{2c}{\pi}\right)^{1/4} \frac{1}{\sqrt{2^n n!}} H_n(x\sqrt{2c}) e^{-cx^2},$$

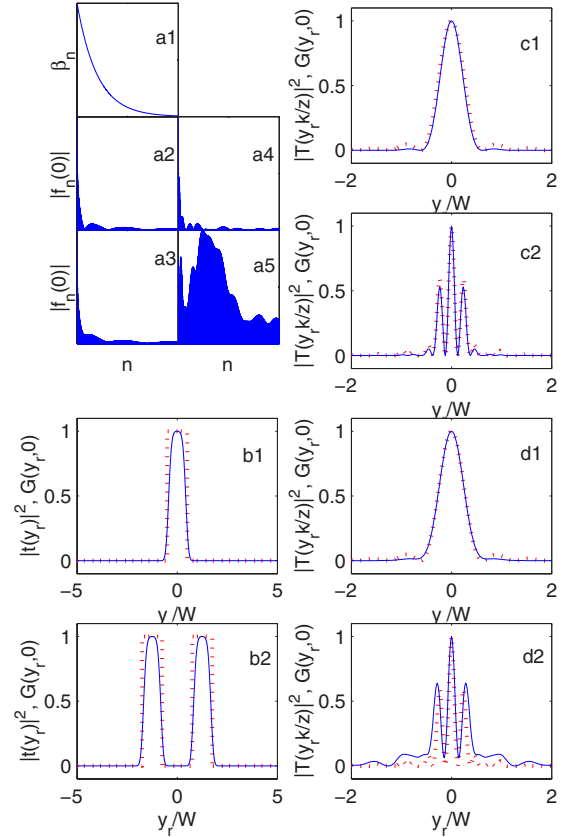


FIG. 2. (Color online) Numerical examples for $q=0.005$ and $a=0.008/W^2$. (a1) The first 1000 eigenvalues β_n . (a2) The first 1000 coefficients $f_n(0)$ of a single-slit object in the ghost imaging and ghost diffractions schemes. (a3) The first 1000 coefficients $f_n(0)$ of a single-slit object in the lensless ghost diffractions schemes. (a4) The first 1000 coefficients $f_n(0)$ of a double-slit object in the ghost imaging and ghost diffractions schemes. (a5) The first 1000 coefficients $f_n(0)$ of a double-slit object in the lensless ghost diffractions schemes. (b1) Ghost imaging of a single-slit. Thick dotted line: the original object $|t(y_r)|^2$; solid line: the image $G(y_r, 0)$. (b2) Ghost imaging of a double-slit. Thick dotted line: the original object $|t(x)|^2$; solid line: the image $G(y_r, 0)$. (c1) Ghost diffraction of a single slit. Thick dotted line: the Fourier transform of the object $|T(y_r, k/z)|^2$; solid line: the image $G(y_r, 0)$. (c2) Ghost diffraction of a double slit. Thick dotted line: the Fourier transform of the object $|T(y_r, k/z)|^2$; solid line: the image $G(y_r, 0)$. (d1) Lensless ghost diffractions of a single slit. Thick dotted line: the Fourier transform of the object $|T(y_r, k/z)|^2$; solid line: the image $G(y_r, 0)$. (d2) Lensless ghost diffractions of a double slit. Thick dotted line: the Fourier transform of the object $|T(y_r, k/z)|^2$; solid line: the image $G(y_r, 0)$.

$$\beta_n = \left(\frac{\pi}{a+b+c}\right)^{1/2} \left(\frac{b}{a+b+c}\right)^n, \quad (10)$$

where $H_n(x)$ are the Hermite polynomials and $a = \frac{1}{4\sigma_s^2}$, $b = \frac{1}{2\sigma_g^2}$, $c = \sqrt{a^2 + 2ab}$. The distribution of β_n is determined by the parameter $q = \sigma_g / \sigma_s$.

In our numerical simulations, we consider two kinds of objects: one is a single slit with the width W ; the other is a double-slit object with the width W and the distance between

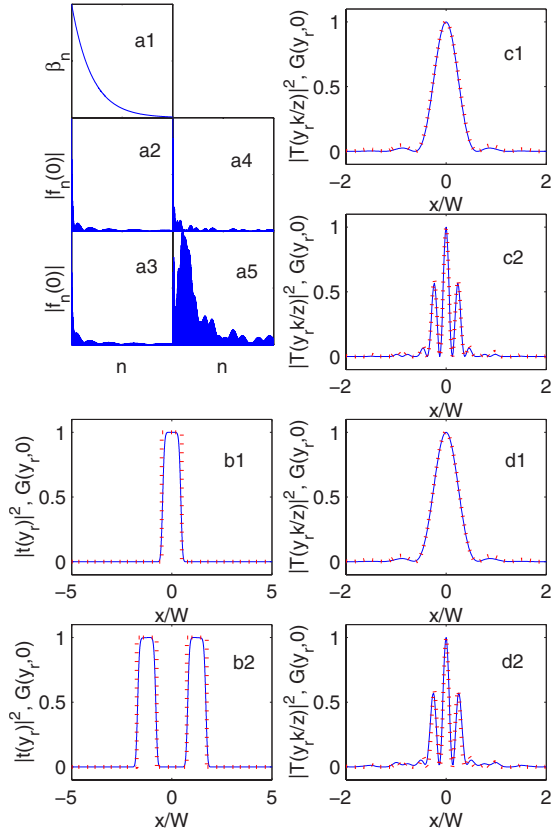


FIG. 3. (Color online) The same as Fig. 2, but $q=0.005$ and $a=0.02/W^2$.

these two slits $1.5W$. So there are three length parameters: W , σ_s , and σ_g . The imaging quality will depend on the ratios between these parameters. From the theory given in Sec. II, we know the images are determined by the distribution of β_n and $f_n(0)$ [Eqs. (6)–(8)]. Since f_n depends on $h_t(x_1, y_t)$ and $\phi_n(x)$, and $\phi_n(x)$ relies on the parameters $\sigma_{s,g}$, all three parameters W , $\sigma_{s,g}$ are important to determine f_n . On the other hand, W does not affect β_n due to Eq. (10). Generally speaking, the level of coherence of the illumination is proportional to σ_g/W .

In Fig. 2, we choose $q=\sigma_g/\sigma_s=0.005$ and $a=0.008/W^2$, then $\sigma_g=0.028W$, $\sigma_s=5.59W$. The distribution of the eigenvalue β_n of the source is shown in Fig. 2(a1). Because $h_t(x_1, y_t)$ is the same in both ghost imaging and ghost diffraction schemes, the corresponding $f_n(0)$ are plotted in Figs. 2(a2) and 2(a4) for the single-slit and double-slit object, respectively. Since β_n has a relative wide distribution, and the distribution of $f_n(0)$ in Figs. 2(a2) and 2(a4) are not very wide, we find the simulated images in the ghost imaging and ghost diffraction schemes are very closed to the standard curves, as shown in Figs. 2(b1), 2(b2), 2(c1), and 2(c2). However, $h_t(x_1, y_t)$ in the lensless ghost diffraction scheme has a different formula. We find the corresponding $f_n(0)$ has a wider distribution, as shown in Figs. 2(a3) and 2(a5), especially for the double-slit object. Thus, in Fig. 2(d2), the differences between the lensless ghost diffraction pattern and the standard curve are very clear.

Generally speaking, if the distribution of β_n is wider than the distribution of $f_n(0)$, one can obtain high quality ghost

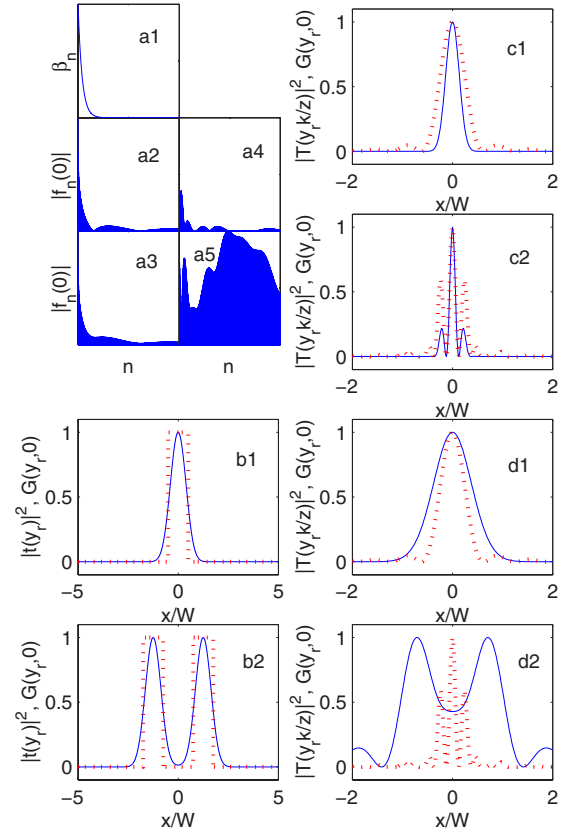


FIG. 4. (Color online) The same as Fig. 2, but $q=0.025$ and $a=0.02/W^2$.

images. On the other hand, if the distribution of $f_n(0)$ is wider than the distribution of β_n , then the ghost images will be significantly degraded. From Eq. (10), when q is much smaller than 1, i.e., σ_s is very large or σ_g is very small, such as an extended highly incoherent source, β_n may have a very wide distribution, then the imaging quality will be improved. Another method to improve the imaging quality is to decrease the distribution of f_n , which can be realized by varying the values of $\sigma_{s,g}$. We use several figures to demonstrate these discussions.

In Fig. 3, we keep $q=0.005$ unchanged, but decrease $\sigma_{s,g}$ so that $a=0.02/W^2$, $\sigma_g=0.0177W$, $\sigma_s=3.5355W$. A source with these parameters is more incoherent than the source used in Fig. 2. Compared with Fig. 2, the distribution of f_n is much narrowed, so the imaging quality is greatly improved. Especially, even the lensless ghost diffraction pattern of the double-slit object is nearly the same as the standard curve, as shown in Fig. 3(d2). Thus, by choosing an appropriate source, we can obtain very perfect images in all three kinds of correlated imaging schemes considered in this paper.

Now, in Fig. 4, we keep $a=0.02/W^2$ unchanged, but set $q=0.025$, then $\sigma_g=0.0884W$, $\sigma_s=3.5355W$. Since σ_g in this case is larger than the values in Figs. 2 and 3, this source is more coherent than the sources used in Figs. 2 and 3. We find the images are significantly degraded. The distribution of β_n is narrowed, and $f_n(0)$ are enlarged at the same time, so there are obvious differences between the simulated patterns and the standard curves. In all our simulations, we find the coefficients $f_n(0)$ in the case of lensless ghost diffraction scheme

have a wider distribution than in the ghost diffraction schemes, so the ghost diffraction has better imaging quality than the lensless ghost diffraction. But if we can make q and σ_g very small, as in the case of Fig. 3, the lensless ghost diffraction also can produce high quality images.

IV. CONCLUSION

In conclusion, we have proposed a method to analyze correlated imaging based on the coherent-mode representation of the partially coherent fields. The correlation function of intensity fluctuations in two detectors can be written as the superposition of many coherent images. The nonlocal image of the object is retrieved from this superposition, and crucially depends on the distribution of the eigenvalues (β_n) of

the coherent-mode representation of the source and the decomposition coefficients ($f_n(0)$) of the objects. When the distribution of β_n is wider than the distribution of $f_n(0)$, high quality ghost images can be obtained. Three kinds of correlated imaging schemes are analyzed numerically. For the Gaussian Schell-model source, decreasing q and σ_g can improve the imaging quality. The eigenvalue distribution can be regarded as a kind of optical transfer function and is very useful in analyzing the imaging quality.

ACKNOWLEDGMENTS

Support from the National Natural Science Foundation of China (Grants No. 10404031 and 60477007), and South China University of Technology is acknowledged.

-
- [1] A. Gatti, M. Bache, D. Magatti, E. Brambilla, F. Ferri, and L. A. Lugiato, *J. Mod. Opt.* **53**, 739 (2006), and references therein.
 - [2] D. V. Strekalov, A. V. Sergienko, D. N. Klyshko, and Y. H. Shih, *Phys. Rev. Lett.* **74**, 3600 (1995).
 - [3] T. B. Pittman, Y. H. Shih, D. V. Strekalov, and A. V. Sergienko, *Phys. Rev. A* **52**, R3429 (1995).
 - [4] B. E. A. Saleh, A. F. Abouraddy, A. V. Sergienko, and M. C. Teich, *Phys. Rev. A* **62**, 043816 (2000).
 - [5] A. F. Abouraddy, B. E. A. Saleh, A. V. Sergienko, and M. C. Teich, *J. Opt. Soc. Am. B* **19**, 1174 (2002).
 - [6] J. Cheng and S. Han, *Phys. Rev. Lett.* **92**, 093903 (2004).
 - [7] A. Gatti, E. Brambilla, M. Bache, and L. A. Lugiato, *Phys. Rev. A* **70**, 013802 (2004).
 - [8] A. Gatti, E. Brambilla, M. Bache, and L. A. Lugiato, *Phys. Rev. Lett.* **93**, 093602 (2004).
 - [9] Y. J. Cai and S. Y. Zhu, *Phys. Rev. E* **71**, 056607 (2005).
 - [10] D. Z. Cao, J. Xiong, and K. G. Wang, *Phys. Rev. A* **71**, 013801 (2005).
 - [11] F. Ferri, D. Magatti, A. Gatti, M. Bache, E. Brambilla, and L. A. Lugiato, *Phys. Rev. Lett.* **94**, 183602 (2005).
 - [12] D. Zhang, Y.-H. Zhai, L.-A. Wu, and X.-H. Chen, *Opt. Lett.* **30**, 2354 (2005).
 - [13] E. Baleine, A. Dogariu, and G. S. Agarwal, *Opt. Lett.* **31**, 2124 (2006).
 - [14] G. Scarcelli, V. Berardi, and Y. Shih, *Appl. Phys. Lett.* **88**, 061106 (2006).
 - [15] L. Basano and P. Ottonello, *Appl. Phys. Lett.* **89**, 091109 (2006).
 - [16] Y. J. Cai and F. Wang, *Opt. Lett.* **32**, 205 (2007).
 - [17] M. Zhang, Q. Wei, X. Shen, Y. F. Liu, H. L. Liu, J. Cheng, and S. S. Han, *Phys. Rev. A* **75**, 021803(R) (2007).
 - [18] L. Mandel and E. Wolf, *Optical Coherence and Quantum Optics* (Cambridge University Press, Cambridge, England, 1995), Secs. 4.7 and 5.5.